International Journal of Thermal Sciences 49 (2010) 1309–1317

Contents lists available at ScienceDirect

International Journal of Thermal Sciences

journal homepage: www.elsevier.com/locate/ijts

Estimation of instantaneous local heat transfer coefficient in spark-ignition engines

A. Mohammadi [a], M. Yaghoubi [b,*]

[a] Mechanical Engineering Department, K. N. Toosi University of Technology, Tehran, Iran
[b] Mechanical Engineering Department, Shiraz University, Shiraz 71348-51154, Iran

ARTICLE INFO

Article history:
Received 2 November 2008
Received in revised form
16 December 2009
Accepted 17 December 2009
Available online 24 February 2010

Keywords:
SI engine
CFD
Heat transfer coefficient
Nusselt number
Combustion
Turbulence
Cylinder head

ABSTRACT

Optimizing heat transfer for internal combustion engines requires application of advanced development tools. In addition to experimental method, numerical 3D-CFD calculations are needed in order to obtain an insight into the complex phenomenas in-cylinder processes. In this context, fluid flow and heat transfer inside a four-valve engine cylinder is modeled and effects of changing engine speed on dimensionless parameters, instantaneous local Nusselt number and Reynolds number near the surface of combustion chamber are studied. Based on the numerical simulation new correlations for instantaneous local heat transfer on the combustion chamber of SI engines are derived. Results for several engine speeds are compared for total heat transfer coefficient of the cylinder engine with available correlation proposed by experimental measurements and a close agreement is observed. It is found that the local value of heat transfer coefficient varies considerably in different parts of the cylinder, but it has equivalent trend with crank angle position.

1. Introduction

Physical processes, which are involved in the combustion chamber of reciprocating engine, are complex. Heat transfer on the wall of a combustion chamber plays an essential role on the behavior of the wall material, engine thermal efficiency and even the emission of NO_x, unburned hydrocarbons as well as knock and their action depend on temperature of in-cylinder gases.

Numerous works have been carried out in the study of heat transfer correlation in reciprocating internal combustion engines [1–10]. Heywood [11] discussed a concise review of engine heat transfer. He summarized results and correlations generated from different studies of various heat transfer mechanisms, spatially, averaged and instantaneous local heat transfer and the effect of each one on the engine performance. His suggested correlations are derived on the hypothesis that Nusselt number could be expressed as a function of Reynolds and Prandtl numbers. It is illustrated that local heat transfer coefficient strongly depends on the local value of Reynolds number. Harigaya et al. [12] estimated instantaneous local heat transfer coefficient on the surface of three types of chambers and the effect of gas flow and flame propagation on the heat transfer coefficient was analyzed. They found a relation between flame velocity and heat transfer coefficient at several positions. Han et al. [13] determined a new empirical formula that predicts instantaneous value of heat transfer coefficient from gas to wall in combustion chamber of an SI engine. Kleemann et al. [14] determined magnitude and origins of local of spatial and temporal surface heat flux variations in a diesel engine using simulation code as well as by experimental measurements. Their investigations revealed that during the early stages of flame impingement on the wall, heat flux undergoes rapid increase by as much as around 10 times the pre-impingement level. These variations can have important consequences for the design of components, especially the piston. Depik and Assanis [15] proposed a universal quasi-steady heat transfer correlation for the intake and exhaust flow of an internal combustion engine. Their correlation developed from the micro scale of turbulence for only one engine-dependent parameter, the Reynolds number. Grau et al. [16] identified combustion parameters and a heat transfer correlation, which verified for an engine at different loads and engine speeds. Zeng et al. [17] used the method of normalizing and reconstructing cylinder pressure in the frequency domain and employed the global heat transfer model proposed by Hohenberg [18] to calculate heat transfer coefficient and heat release in a combustion chamber.

* Correspondence to: M. Yaghoubi, Academy of Sciences, Islamic Republic of Iran. Tel.: +98 711 6474614; fax: +98 711 2301672.
E-mail address: yaghoub@shirazu.ac.ir (M. Yaghoubi).

1290-0729/$ – see front matter © 2009 Elsevier Masson SAS. All rights reserved.
doi:10.1016/j.ijthermalsci.2009.12.010

Nomenclature

ATDC	after top dead center
A_0	zero in laminar calculation and unit for turbulent model
a	dimensionless quantity
B	diameter of cylinder (m)
BTDC	before top dead center
BDC	bottom dead center
$c_{\varepsilon_1}, c_{\varepsilon_2}, c_{\varepsilon_3}, \mathrm{Pr}_k, \mathrm{Pr}_\varepsilon, c_\mu$	constants
c_p	specific heat at constant pressure (kJ kg^{-1} K^{-1})
D	Ficks law diffusion coefficient (m^2 s^{-1})
F^s	rate of momentum gain per unit volume due to spray (kg s^{-1} m^2)
g	specific body force (gravity) (m s^{-2})
h	heat transfer coefficient (W m^{-2} K^{-1})
h_m	specific enthalpy of species m (kJ kg^{-1})
I	specific internal energy (kJ kg^{-1})
J	diffusion flux (kJ)
K	thermal conductivity (W m^{-1} K^{-1})
k	turbulent kinetic energy (m^2 s^{-2})
L	stroke (m)
n	normal direction to cylinder head
Nu	Nusselt number
p	fluid pressure (kPa)
$\dot{Q}^c$	source term due to chemical heat release (kJ mol^{-1})
$\dot{Q}^s$	source term due to spray interaction (kJ mol^{-1})
R	crank radius (m)
r_c	compression ratio
Re	Reynolds number
rpm or N	revolution per minutes
SI	spark-ignition engine
T	temperature (K)
T_g	gas temperature of first grid from the wall (K)
T_w	temperature of the cylinder head (K)
TDC	top dead center
u	fluid velocity vector (m s^{-1})
v	actual local gas velocity (m s^{-1})
v_m	mean piston speed (m s^{-1})
w	defined velocity for Woschni correlation (m s^{-1})
$\dot{W}^s$	source term due to interaction with spray (kJ kg^{-1})
z	axial cylinder length (m)

Greek symbols

ε	turbulent dissipation rate (m^2 s^{-3})
δ	Dirac delta function
κ	Karmann's constant
ρ_m	mass density of species m (kg m^{-3})
ρ	total mass density (kg m^{-3})
$\dot{\rho}^c_m$	source term due to chemistry (kg m^{-3})
$\dot{\rho}^s$	source term due to spray (kg m^{-3})
σ	viscous stress tensor (kPa)
∇	gradient operator
θ	crank angle
μ	dynamic viscosity (kg m^{-1} s^{-1})

Mohamadi et al. [19] investigated heat flux, heat transfer coefficient on the cylinder head, cylinder wall, piston, and intake, and exhaust valves with respect to crank angle position. They suggested new correlations to predict maximum and minimum convective heat transfer coefficient in the combustion chamber of an SI engine.

In recent years, computational fluid dynamics (CFD) as a rapid and cost effective tool is being increasingly used in different stages of engine design and optimization, and it can be utilized to find heat transfer coefficient at various positions in an engine cylinder. The purpose of this study is to model fluid flow and heat transfer inside a four-valve SI engine cylinder. The effect of variation in the engine speed on dimensionless parameters, instantaneous local Nu and Re numbers near the wall surface of combustion chambers is studied and correlations for instantaneous local heat transfer on the combustion chamber of SI engines are derived. Such results of local variation of heat transfer with crank angle positions are very important for the analysis of thermal problem of SI engines, such as stress analysis and cooling system of SI engines.

2. Governing equations

The CFD code that is employed for heat transfer calculations uses a high Reynolds number turbulence model in conjunction with law-of-the-wall to describe near the wall flow conditions and reducing the computation time [20]. The three dimensional compressible averaged Navier–Stokes equations are solved on a moving mesh and turbulent fluxes are modeled by an eddy viscosity concept, using κ–ε model.

2.1. Fluid flow

The equations of motion for the fluid phase are used to solve both laminar and turbulent flows. The equations of mass, momentum and energy for two cases differ primarily in the form and magnitude of transport coefficients (i.e., viscosity, thermal conductivity, and species diffusivity) which are much larger in the turbulent case. For turbulent flows, transport coefficients are derived from a turbulent diffusivity that depends on the turbulent kinetic energy and its dissipation rate. The continuity equation for species m is:

$$\frac{\partial \rho_m}{\partial t} + \nabla\cdot(\rho_m u) = \nabla\cdot\left[\rho D \nabla\left(\frac{\rho_m}{\rho}\right)\right] + \dot{\rho}^c_m + \dot{\rho}^s \delta_{m1} \tag{1}$$

Where diffusion according to Ficks law is being assumed. The momentum equations for fluid mixture are:

$$\frac{\partial(\rho u)}{\partial t} + \nabla\cdot(\rho u u) = -\frac{1}{a^2}\nabla p - A_0 \nabla\left(\frac{2}{3}\rho k\right) + \nabla\cdot\sigma + F^s + \rho g \tag{2}$$

The dimensionless quantity a is used in conjunction with the Pressure Gradient Scaling (PGS) method [7,21]. This is a method for enhancing computational efficiency in low Mach number flows, where the pressure is nearly uniform.

2.2. Turbulence model

For turbulence modeling $A_0 = 1$, and two additional transport equations are needed to be solved one for the turbulent kinetic energy κ and second for its dissipation rate ε:

$$\frac{\partial \rho k}{\partial t} + \nabla\cdot(\rho u k) = -\frac{2}{3}\rho k \nabla\cdot u + \sigma : \nabla u + \nabla\cdot\left[\left(\frac{\mu}{\mathrm{Pr}_k}\right)\nabla k\right] - \rho\varepsilon + \dot{W}^s \tag{3}$$

$$\frac{\partial \rho \varepsilon}{\partial t} + \nabla\cdot(\rho u \varepsilon) = -\left(\frac{2}{3}c_{\varepsilon_1} - c_{\varepsilon_3}\right)\rho\varepsilon\nabla\cdot u + \nabla\cdot\left[\left(\frac{\mu}{\mathrm{Pr}_\varepsilon}\right)\nabla\varepsilon\right] + \frac{\varepsilon}{k}\left[c_{\varepsilon_1}\sigma : \nabla u - c_{\varepsilon_2}\rho\varepsilon + c_s \dot{W}^s\right] \tag{4}$$

The source term $(c_{\varepsilon_3}-\frac{2}{3}c_{\varepsilon_1})\nabla\cdot u$ accounts for length scale change and $\dot{W}^s$ arise due to interaction with spray. The quantities $c_{\varepsilon_1}, c_{\varepsilon_2}, c_{\varepsilon_3}, \mathrm{Pr}_k$ and Pr_ε are constant whose values are determined from experiments and some theoretical considerations [22].

Internal energy equation is:

$$\frac{\partial(\rho I)}{\partial t}+\nabla\cdot(uI) = -p\nabla\cdot u+(1-A_0)\sigma:\nabla u-\nabla\cdot J +A_0\rho\varepsilon+\dot{Q}^c+\dot{Q}^s \quad (5)$$

where:

$$J = -K\nabla T-\rho D\sum_m h_m\nabla\left(\frac{\rho_m}{\rho}\right) \quad (6)$$

and I is the specific internal energy, exclusive chemical energy, and J is the contribution due to heat conduction and enthalpy diffusion.

2.3. Law-of-the-wall

In engine calculations, ordinary uses turbulent law-of-the-wall velocity condition with fixed temperature walls. For turbulent law-of-the-wall conditions the tangential components are determined by matching to logarithmic profile:

$$\frac{v}{u^*}=\begin{cases}\frac{1}{\kappa}Ln\left(c_{lw}\varsigma^{7/8}\right)+B & \varsigma>R_c\\ \varsigma^{1/2} & \varsigma<R_c\end{cases} \quad (7)$$

Where: $\varsigma=\rho y v/\mu_{\mathrm{air}}(T)$ is the Reynolds number based on the gas velocity relative to the wall which is evaluated at distance y from wall, and u^* is the shear speed, it is assumed that y is small enough to be in the laminar sublayer region of the turbulent boundary layer. The R_c defines the boundary between these two regions. The constant κ, c_{lw}, R_c and B are related to κ–ε model constant by:

$B=5.5$, $c_{lw}=0.14$, $\kappa=0.437$, $R_c=114$ that commonly accepted values of the κ–ε constants.

For fixed temperature walls using the turbulent law-of-the-wall condition, J_w is determined from the modified Reynolds analogy formula:

$$\frac{J_w}{\rho u^* c_p(T-T_w)}=\begin{cases}1/\left(\mathrm{Pr}_{\varepsilon}\frac{v}{u^*}\right) & \varsigma\le R_c\\ 1/\left\{\mathrm{Pr}\left[\frac{v}{u^*}+\left(\frac{\mathrm{Pr}_l}{\mathrm{Pr}}-1\right)R_c^{1/2}\right]\right\} & \varsigma>R_c\end{cases} \quad (8)$$

T_w is the wall temperature and Pr_l is the Prandtl number of the laminar fluid.

2.4. Combustion

The combustion model is Spalding's eddy-breakup model [23,27]. Spalding suggested that combustion processes are best understood by focusing attention on coherent bodies of gas, which squeezed and stretched during their travel through the flame. This model relates the local and instantaneous turbulent combustion rate to the fuel mass fraction and the characteristic time scale of turbulence. The application of this model requires adjustment of a specific coefficient and spark time to match the experimental combustion rate with the computational combustion rate. In spark-ignition engine combustion chamber, high turbulence intensity exists and hence combustion for such device lies in the flamelets-in-eddies regime. The intrinsic idea behind the eddy-breakup model is that the rate of combustion is determined by the rate at which parcel of unburned gas is broken down into the smaller ones. Such that there is sufficient interfacial area between the unburned mixture and hot gases to permit reaction and also the quit important turbulence length scale is determined by turbulent burning rates.

Table 1
The engine specifications.

Bore	85 mm
Stroke	88 mm
Compression ratio	10.3
Engine Speed	3500 rpm
Displacement volume	1997.5 cm^3
Intake valve opening	22 BTDC
Intake valve closing	62 BTDC
Exhaust valve open	116 ATDC
Exhaust valve close	28 ATDC
Fuel	Gasoline
Equivalence ratio	1.1
Spark time	17 BTDC

3. Mesh preparation

The engine specification is presented in Table 1. The engine combustion chamber has four inclined valves and one bowl in piston as shown in Fig. 1.

Prior to CFD simulation, computational mesh was generated for the engine using Gambit scheme. The geometry of a mesh is composed of any arbitrary number of logical blocks that are patched together in a seamless fashion. Patching allows complex geometries to be created, block by block while minimizing the number of deactivated zones that surround the final mesh. The movement of piston/flow domain was resolved using the boundary motion feature of available code. During the solution process, as the piston moves, the internal mesh structure deforms automatically to optimize the mesh. The distortion of each individual cell occurs when the generated cell distortion reaches a certain level, and the solution is re-zoned onto new mesh.

Mesh size ranged from about 90 000 at BDC to about 46 000 at TDC for computational studies. Fig. 1 shows the geometry and grid configuration of the engine. In Table 2, variations of grid and maximum pressure in a full cycle are presented. This table illustrates that the solutions are mesh independent because with increasing grids from 84 000 to 90 000 no variation is observed in the pressure profiles.

4. Initial and boundary conditions

Computation starts at TDC. Initial charge densities were calculated based on ambient pressure of 0.80 bar and temperature of 300 K at inlet valves, opening. The standard κ–ε turbulence model in the code was used with an initial value of turbulent kinetic

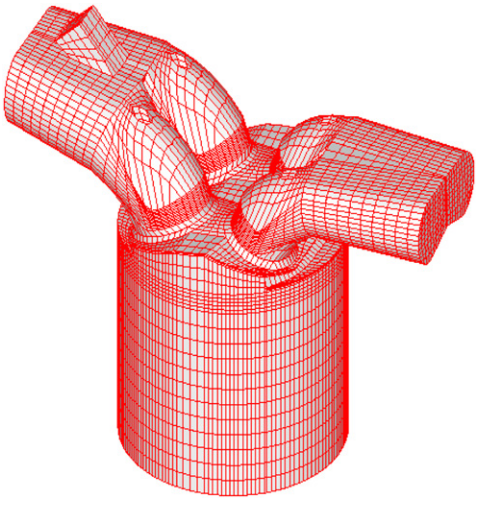

Fig. 1. Mesh for the CFD calculation.

Table 2
Variations of maximum pressure with mesh size.

Mesh size at bottom dead center	Maximum pressure in cycle	Crank angle of maximum pressure
51 000	3.60 MPa	381°
60 000	4.10 MPa	380°
71 000	4.40 MPa	377°
84 000	4.79 MPa	377°
90 000	4.79 MPa	377°

energy k, assumed 10% of the total kinetic energy based on the mean piston speed that assumed to be uniform. Radial velocity is initialized assuming a swirl ratio 0.0. Temperature was taken as 485 K for liner, 600 K for cylinder head and piston, 550 K for intake valves, and 800 K for exhaust valves.

5. Basic relations

Dimensional analysis can be used to develop the functional form of relations, which govern the gas-side heat transfer coefficient. The engine convective heat-transfer process can be characterized geometrically by a length dimension-say the bore B- and a number of length ratios y_1, y_2, y_3, etc. of which, one will be the axial cylinder length z divided by the bore z/B, which defines the cylinder and combustion chamber geometry. The flow pattern, similarly, may be characterized by one chosen velocity v and set of velocity ratios u_1, u_2, u_3, etc. The gas properties of importance are thermal conductivity k, the dynamic viscosity μ, the specific heat c_p and the density ρ. If there is combustion, then the chemical energy release rate per unit volume $\dot{q}_{ch}$ may be important. The engine speed N and the relative position in the cycle denoted by crank angle θ introduce the cyclical nature of the process. Thus:

$$f(h, B, s, y_1, \ldots, y_m, v, u_1, \ldots, u_m, k, \mu, c_p, \rho, q, N, \theta) = 0.0 \tag{9}$$

Applying dimensional analysis reduces the variables to some non-dimensional groups:

$$F\left(\frac{hB}{k}, \frac{\rho v B}{\mu}, \frac{c_p \mu}{k}, \frac{c_p T}{v^2}, \frac{NB}{v}, \frac{q}{\rho c_p N T}, \frac{s}{B}, y_1, \ldots, y_m, u_1, \ldots, u_n, \theta, k, \mu, c_p, \rho, q, N, \theta\right) = 0.0 \tag{10}$$

The first three groups are the familiar Nu, Re, and Pr numbers, respectively. The next has the nature of a Mach number since c_pT is proportional to the square of the sound speed, for Mach number much less than one, the Mach number dependence is known to be small and can be omitted. It is usual to take for v the mean piston speed because in the experiments, it is too difficult to determine the spatial velocity factors but, with CFD, we can use actual velocity and do not need to use such simplifications. Then by introducing the bore/stroke ratio, the term NB/v is eliminated. The ratio of S/B is a function of the compression ratio r_c, the ratio of connecting rod to crank radius $R = l/a$ and θ. Thus:

$$f\left(\frac{hb}{k}, \frac{\rho v b}{\mu}, \frac{c_p \mu}{k}, \frac{b}{L}, \frac{\dot{q}_{ch}}{\rho c_p N T}, r_c, R, y_1, \ldots, y_m, \theta, u_1, \ldots, u_n\right) = 0.0 \tag{11}$$

Finally, the basis of these correlations is the assumption that the Nu, Re, and Pr number relation-ship follows that found for steady turbulent flow in pipes or flat plates [11]. The geometric comparison of cylinder and the tube suggests their heat-transfer processes involving fluid may be similar to:

$$\mathrm{Nu} = a\mathrm{Re}^m \mathrm{Pr}^n \tag{12}$$

Where: $\mathrm{Nu} = hB/k$ and $\mathrm{Re} = \rho v D/\mu$ which contains few zero dimensional term and a, m, n are undetermined constants. Nu involves the heat transfer coefficient, Re is an expression of zero dimensional flow velocity, and Pr is the ratio of heat and molecular diffusion. The Pr number usually consider constant when the fluid is gas so that the influence of the Prandtl number will be small, since the Pr number will be approximately constant. For gases, relation (12) reduced to the following:

$$\mathrm{Nu} = a\mathrm{Re}^m \tag{13}$$

From computation instantaneous fluid properties v, μ, k, ρ, h for each point of grid can be determined. Thus, dimensionless parameters Nu and Re for the flow are determined. With getting natural logarithm from both side of Eq. (13), we have:

$$Ln\mathrm{Nu} = mLn\mathrm{Re} + Lna \tag{14}$$

This equality shows that the graph *of* $Ln(\mathrm{Nu})$ vs. $Ln(\mathrm{Re})$ is a line that slope of it is m and intercept of it is $Ln(a)$ and hence a, m can be determined and correlation for each location would be determined. A log–log plot of Nu vs. Re is first made for one field to estimate the dependence of the heat transfer on the Reynolds number, i.e. to find an approximate value of the exponent m.

6. Thermal transfer to the wall

In the case of $\mathrm{Nu} = f(\mathrm{Re})$, only mode of convection heat transfer considered in this paper because, almost all the values of productions of combustion are water vapor and carbon dioxide, that have very little value of emissivity and hence, radiation heat transfer is very small compare to convection heat transfer analysis in Spark-Ignition engine and can be ignored.

For any of three locations, we delivered four correlations, intake, before arrival of the flame, after arrival of the flame and exhaust processes. In the intake process, mixture contains fuel and air, and velocity (Re number) of them, is due to vortex that is generated because of opening of intake valves and upward movement of piston. In exhaust processes, velocity of productions is due to the diffusion of the turbulence flame in-cylinder mixture and hence, there is considerable difference between velocity (Re number) in these two processes. In two processes, (intake and exhaust) mean temperature of gases has considerable difference value because of heat release of combustion and hence we have two different values for heat transfer coefficient. With arrival of the flame to a location, there is seen a jumping in temperature and in this time due to flame propagation, vector of gas velocity and flame direction become opposite to each other and after arrival of the flame to a location, it is seen intense loss in velocity value (Re number).

7. Validation

To validate the computational scheme and the numerical method, total heat transfer on the combustion chamber (averaging on cylinder head, cylinder wall, piston, and intake and exhaust valves) near the spark time of engine is determined and compared with Woschni's correlation [24]:

$$h = 3.26 B^{-0.2} p^{0.8} T^{-0.55} w^{0.8}, \quad \mathrm{W/m^2K} \tag{15}$$

Where B is diameter of piston in m, p is average gas velocity in kPa, T is temperature in Kelvin and w is the average gas velocity in m/s. Woschni correlation is the most popular correlation for determining, overall heat transfer coefficient that is accepted by many researchers and hence we use it to validate our results. The other correlations are not accepted by most of the researchers. Results are illustrated in Fig. 2 for several engine speeds. A very good

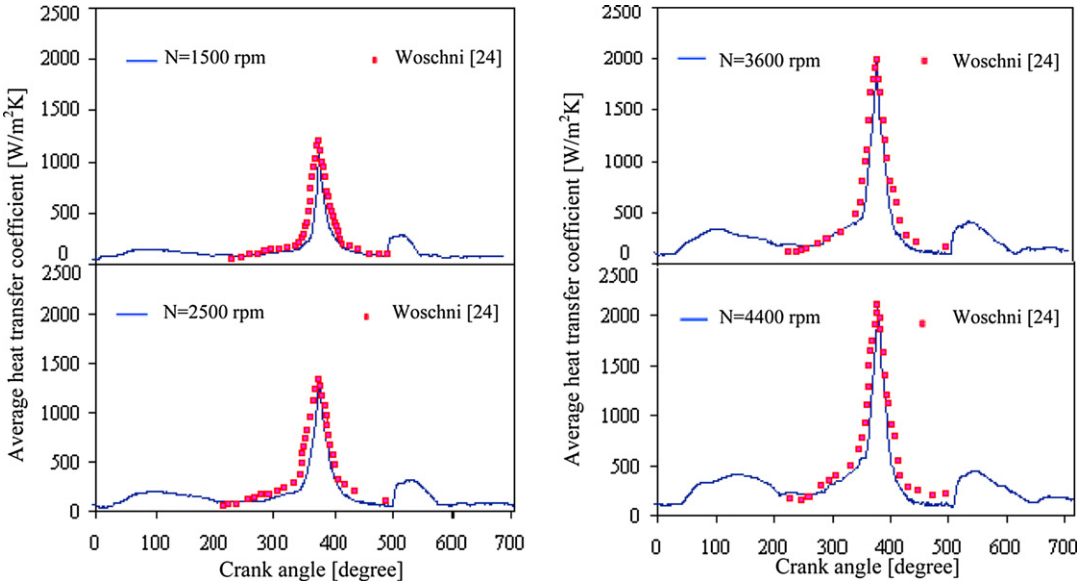

Fig. 2. Comparison of heat transfer coefficient on the combustion chamber with Woschni's correlation at various speed (1500, 2500, 3600 and 4400 rpm).

agreement can be observed between the present computation and Woschni's correlation. Eq. (15) predicts the average value of heat transfer coefficient correctly but do not accurately predict the value of heat transfer in the intake or exhaust process as we discussed in [19].

In Fig. 4 comparison between experimental and calculated mean gas temperature is shown [25]. In Fig. 5-a contour of temperature in mid vertical plane at 10° ATDC is shown. In the red region burned gases is seen and average temperature is about 2500 K. In Fig. 5-b, experimental flame propagation that is measured by Taylor et al. [26] was shown. CFD simulation was done with the same condition as in their paper. These two figures have good corresponding with each other.

8. Results

In Fig. 3 locations on the combustion chamber surface within the cylinder head selected for further investigation are illustrated. Radial locations situated on the engine head at cylinder axis, were 13 and 26 mm from the cylinder axis. These points referred from 1 to 3 in this study.

The complete full cycle is divided into four different processes, intake, before arrival of flame, after arrival of the flame, exhaust that is shown in Fig. 6. The values of instantaneous local Nu and Re numbers are shown in Figs. 7 and 8. The engine speed is changed from 1500 rpm to 4400 rpm and for each speed, the corresponding instantaneous value of Re during a full cycle is illustrated in Fig. 6. As the speed of engine increases, the larger is the local Re number. For each speed, there is a maximum variation in the intake and minimum variation at the exhaust. Point 2 on the cylinder head has the highest adjacent gas velocity and point 3 has the lowest nearby gas velocity.

One of the most important variables that affect the magnitude of heat transfer is the engine speed. With increasing engine speed, velocity of gas inside the cylinder increases and the result enhances the turbulence intensity of flow and heat transfer coefficient. In this context, effect of engine speed (versus engine revolution, mean piston speed is defined by $v_m = 2LN/60$) on the local value of Nu and Re numbers in a full cycle is investigated. Then the logarithmic graphs of Nu vs. v_m and Re vs. v_m individually are drawn in Figs. 6 and 7. Elimination of v_m between two graphs, will result the correlation of Ln(Nu) vs. Ln(Re).

Based on the definition of $h = (-K\partial T/\partial n)_w/(T_w - T_g)$ and $\mathrm{Nu} = hB/K$, the value of Nusselt number is determined during full cycle for various points 1, 2, and 3 from 1500 rpm to 4400 rpm. Where T_g is the temperature of first grid from the wall and not the mean temperature, T_w is the temperature of cylinder head, K is the thermal conductivity, n is the direction normal to the surface of

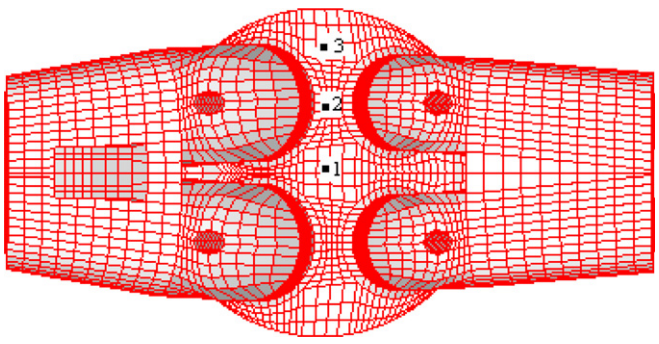

Fig. 3. Specific locations on the cylinder head considered.

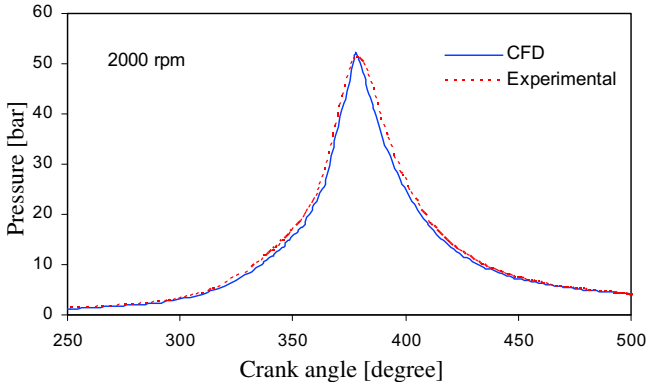

Fig. 4. Comparison between experimental and calculated mean cylinder pressure in 2000 rpm [25].

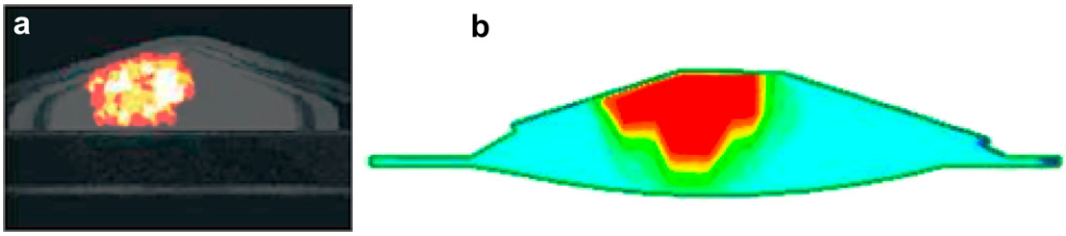

Fig. 5. (a): Contour of temperature at 10° ATDC from simulation (b): Flame propagation at 15° ATDC [26].

cylinder head in those points and $(\partial T/\partial n)_w$ is the temperature gradient on the cylinder head in direction of the n. For all three points, maximum convection takes places during flame propagation. Although Re is lower at point 3 but convection is the highest at that location which is close to flame. Heat transfer takes places before and after flame and convection is negligible during intake and exhaust processes.

Details of the four processes in a full cycle are shown in Figs. 7 and 8. These figures illustrate that:

1. *Start of cycle (TDC) until closing the intake valves*: From TDC and entering of air and fuel mixture (intake valves opened 22 crank angle BTDC) vortex is setup in the cylinder and velocity (Re) near the surface of combustion chamber increases and reaches to two relative maximum. The value of one of the maximum value changes due to spray of fuel and crank angle of maximum for all points, the next maximum part is due to maximum mean piston speed that occur 90 crank angle ATDC. After moving down the piston, damping of vortex and decreasing of turbulence intensity, velocity (Re) is decreased and this reduction continues until BDC. After 180 crank angle, with almost 5–10 crank angle difference (the time that effect of moving up the piston causes vortex become strong), velocity (Re) near the surface of combustion chamber increases and then near the time of closing the intake valves due to the end of spray, velocity continues to decrease.
2. *From closing of intake valves up to flame arrival*: With compression of mixture due to upward movement of piston, and vortex that initiate from spray in the intake process, velocity (Re) increases near the combustion chamber and at the end of compression process increases the density of mixture cause the increase of Re.
3. *From arrival of the flame up to opening exhaust valves*: the time of arrival of flame for various points are different, point 1 almost 10 crank angle, point 2 almost 20 crank angle and point 3 almost 30 crank angle after spark time. With arrival of flame

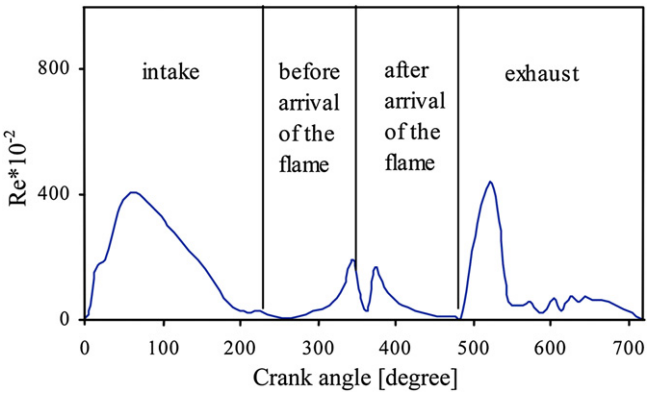

Fig. 6. Four processes of a full cycle for instantaneous investigation.

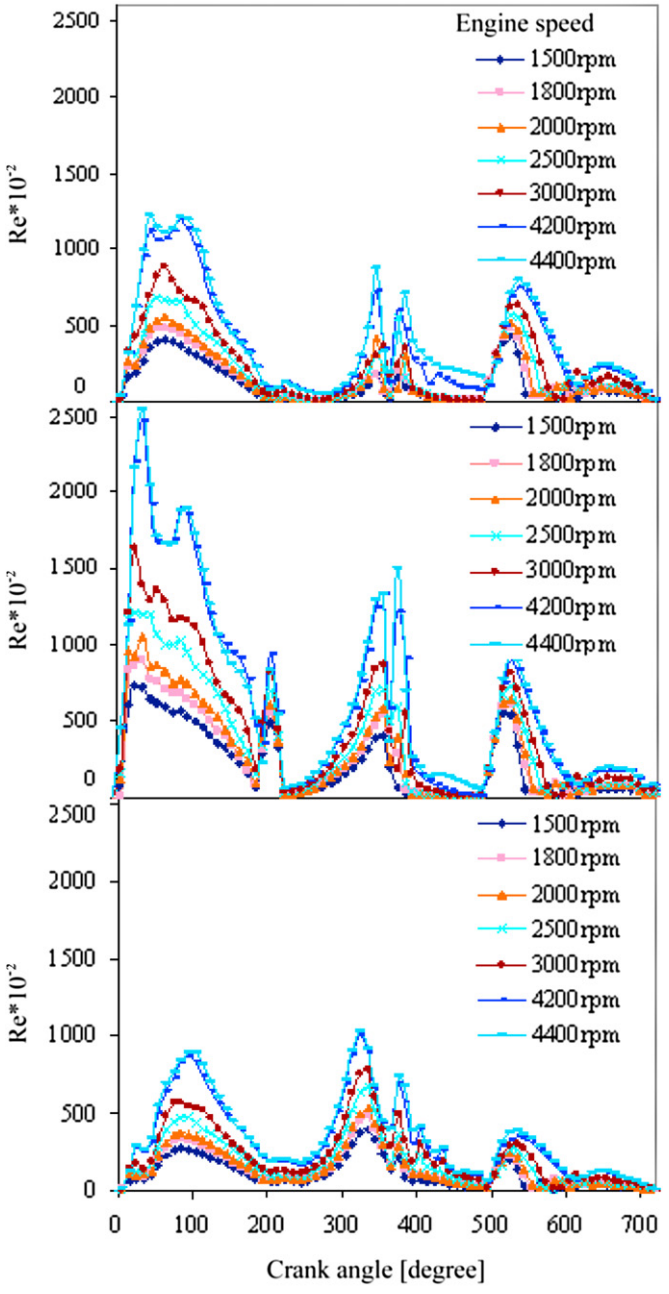

Fig. 7. Variation of Reynolds number at some locations on the combustion chamber surface with crank angle.

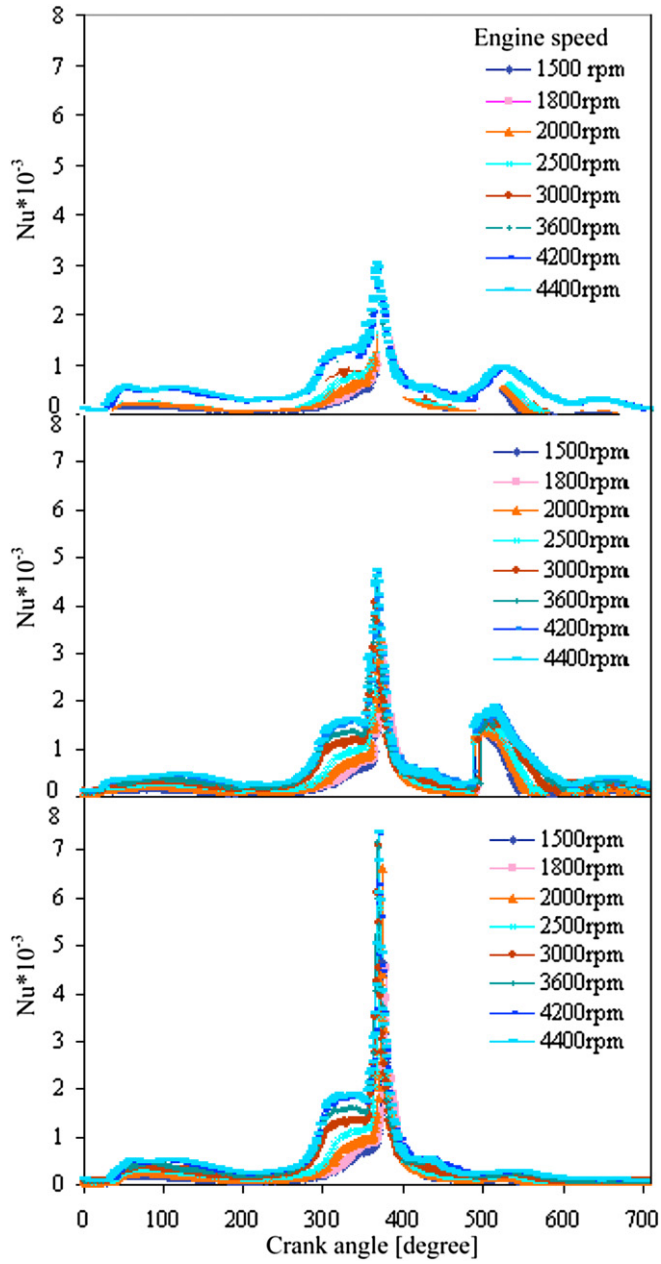

Fig. 8. Variation of heat transfer coefficient on some locations of the combustion chamber surface with crank angle.

to each point and jumping of gas temperature (most of the gases of cylinder is nitrogen and $\mu \propto T^{0.62}$ [11]) coefficient of viscosity increases. Moreover, due to the direction of vortex and flame diffusion that are opposite of each other, velocity of gases decrease and Re also decreases. Then with high velocity of flame diffusion inside the combustion chamber, Re increases. With expansion of gases, as the effect of kinetic energy losses, the pressure and temperature loss, the value of velocity in each point decreases, gas density also decreases and hence corresponding Re decreases too.

4. *From opening of exhaust valves to TDC that cycle finished*: In the end of expansion process with opening of exhaust valves hot gases of combustion due to difference of pressure between inside cylinder and outside cylinder, leave the combustion chamber with high velocity. This effect causes that velocity (Re) increases inside combustion chamber. With exhaust of hot gases of combustion and high decrease in pressure difference between inside cylinder and environment, velocity (Re) decreases near the combustion chamber; until TDC the value of Re oscillates but it nearly has constant value.

Heat transfer coefficient is function of velocity near the combustion chamber wall and Nu has direct correlation with heat transfer coefficient. Due to this variation, Nu is function of local velocity of inside cylinder. With increase and decrease of velocity in the intake processes, increase or decrease in the value of Nu are

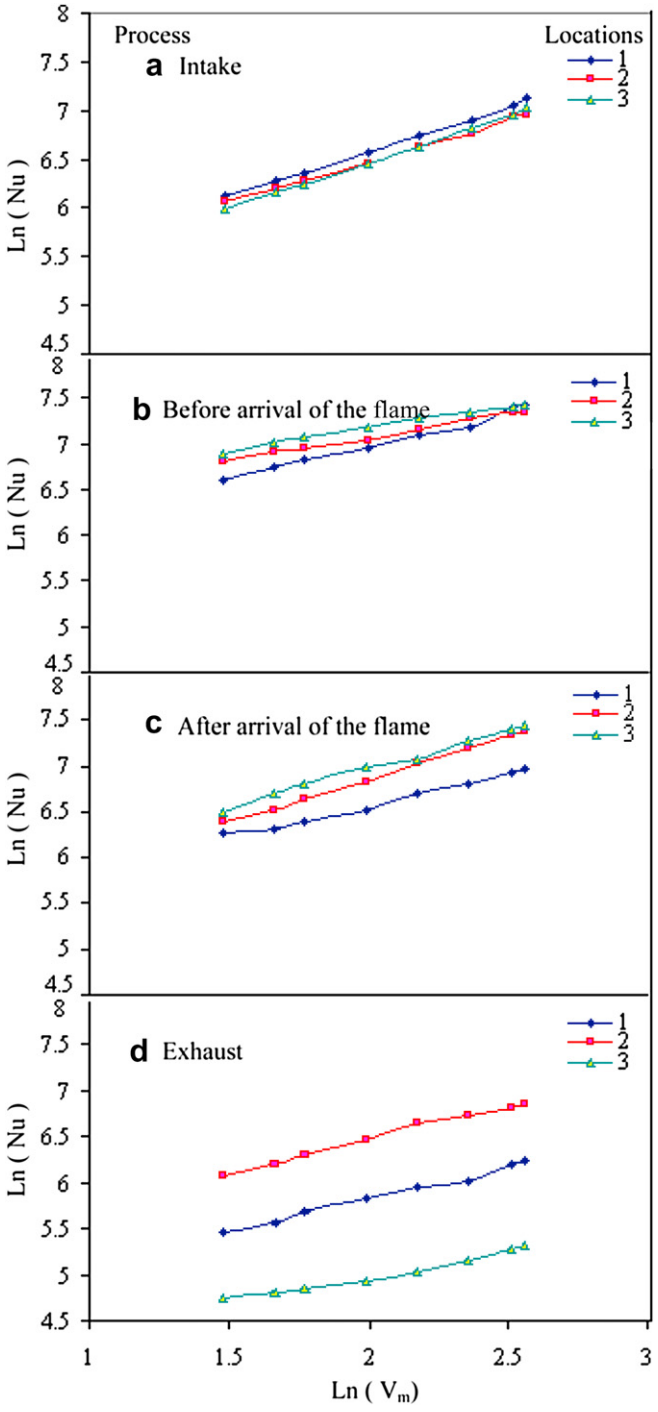

Fig. 9. Variation of Ln(Nu) vs. $Ln(v_m)$ for processes1 1–4 (a–d).

observed. For in-cylinder gases (most of the gases of cylinder is nitrogen and $K \propto T^{0.62}$ [11]) and with arriving of flame, jumping in thermal conductivity is seen and due to this Nu has high reduction in its value that causes instantaneously decrease in Nu number.

9. Convection correlations

In Figs. 9 and 10 the logarithmic graphs of Nu and Re vs. mean piston speed, are plotted individually. With elimination of logarithm from mean piston speed, relation between Nu vs. Re will be available and corresponding correlations for heat transfer inside cylinder will be determined. For each process the mean value of Nu and Re are determined and presented as follows:

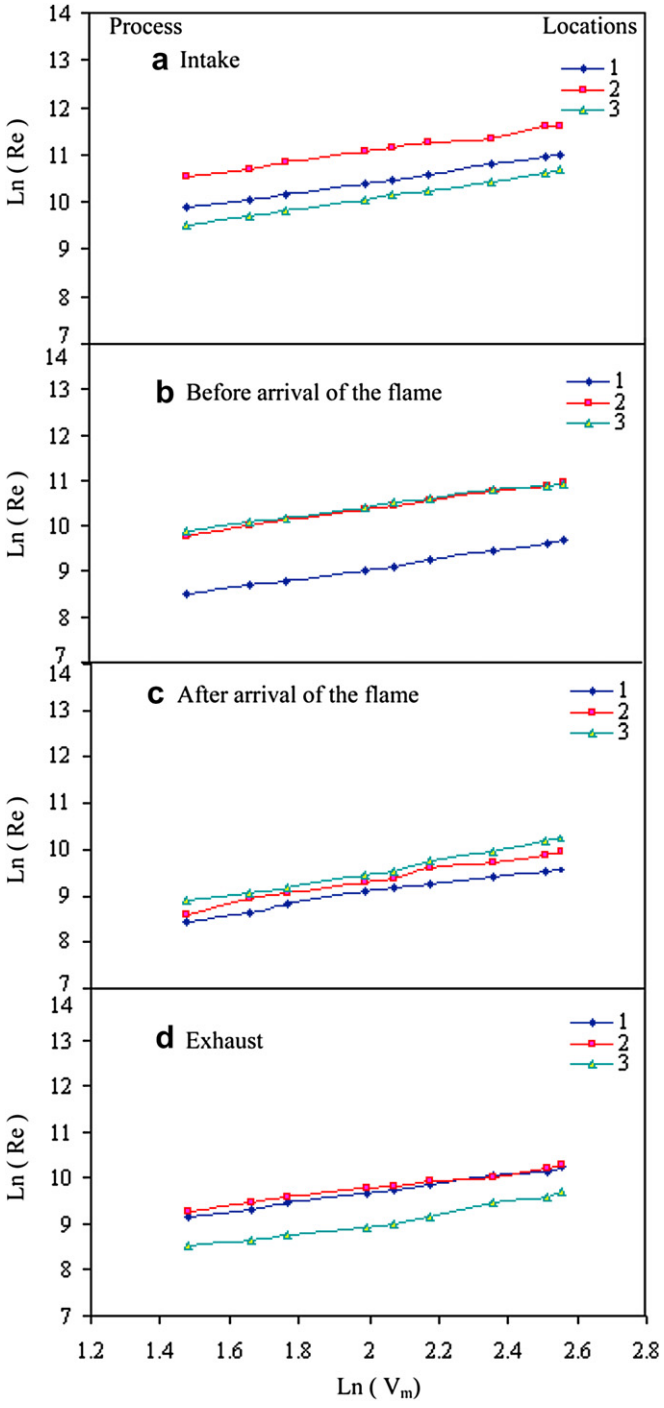

Fig. 10. Variation of $Ln(\mathrm{Re})$ vs. $Ln(v_m)$ for processes1 1–4 (a–d).

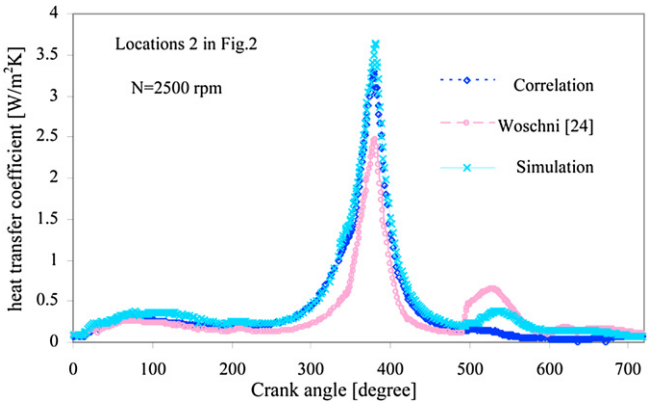

Fig. 11. Comparison of local heat transfer coefficient (location 2) with Woschni's correlation at the same position.

Location 1:
- Process I) $Nu = 0.084Re^{0.87}$
- Process II) $Nu = 2.1Re^{0.69}$
- Process III) $Nu = 2.1Re^{0.64}$
- Process IV) $Nu = 0.32Re^{0.72}$

Location 2:
- Process I) $Nu = 0.052Re^{0.85}$
- Process II) $Nu = 8.28Re^{0.48}$
- Process III) $Nu = 0.66Re^{0.78}$
- Process IV) $Nu = 0.21Re^{0.82}$

Location 3:
- Process I) $Nu = 0.09Re^{0.88}$
- Process II) $Nu = 7.8Re^{0.49}$
- Process III) $Nu = 2.37Re^{0.64}$
- Process IV) $Nu = 1.91Re^{0.48}$

Heat transfer correlation inside pipe with turbulent flow is $Nu = 0.023Re^{0.8}Pr^{0.4}$, which has good agreement with intake process correlation [19].

Fig. 11 illustrates a comparison between (three graphs) the local heat transfer coefficient for location 2 that calculated using CFD simulation in 2500 rpm and correlation for point 2 and area averaged heat transfer coefficient predicted by Woschni's correlation. It should be noted that these three graphs have the same value in intake and start of compression process but after combustion period have different values with each other and correlation 2 predict a better value for heat transfer coefficient than Woschni's correlation. There is not any local correlation to justify correlation 2 and hence we tried to give correlation for determining local heat transfer coefficient.

10. Conclusions

Instantaneous local values of Nu and Re number on the combustion chamber in an SI engine were computed using CFD code. The effect of engine speed on the local variations of these dimensionless parameter were investigated for various engine speed. As a result, the following conclusions were derived:

1) The time when surface temperature rises is related to its flame arrival time at each position.
2) With increasing engine speed the values of Nu and Re increase too.

3) A substantial difference of the value of Re and Nu exists for various location in the cylinder head of SI engines.
4) Various correlations in form of $Nu = aRe^m$ to predict heat transfer coefficient for different locations on the cylinder head for each process are proposed during a full engine cycle.
5) Total heat transfer coefficient calculated is in agreement with available correlation, proposed for SI engines.

References

[1] G. H. Abd Alla, Computer Simulation of a Four-stroke Spark Ignition Engine, SAE Paper, No. 2001-01-0578, 2001, pp. 1–11.
[2] C.R. Fergusen, Internal Combustion Engines-applied Thermoscience, second ed. John Wiley & Sons, New York, 2003, pp. 230–244.
[3] A. Jafari, S.K. Hannani, Effect of fuel and engine operational characteristics on the heat loss from combustion chamber surfaces of SI engines. International Communication in Heat and Mass Transfer 33 (2006) 122–134.
[4] S. Etemad, C.F. Stein, S. Erilksson, Heat Transfer Analysis and Averaged Heat Flux Prediction by Means of CFD and its Validation for an IC-engine, SAE Paper, No 2005-01-2029, 2005.
[5] A.R. Noori, M. Rashidi, Computational fluid dynamics study of heat transfer in a spark-ignition engine combustion chamber. ASME Journal of Heat Transfer 129 (2007) 609–616.
[6] A. Mohammadi, A. Jazayeri, M. Zbasharhagh, Numerical simulation of convective heat transfer in a spark ignition engine, in: Proceedings of ICE Division of ASME, Spring Technical Conference, Chicago, Illinois, USA, 2008.
[7] A. Sorin, F. Bouloc, B. Bourouga, P. Antoine, Experimental study of periodic heat transfer coefficient in the entrance region of exhaust pipe. International Journal of Thermal Science 47 (2008) 1665–1675.
[8] A. Sharief, T.K. Chandrashekar, A.J. Antony, B.S. Samaga, Study on Heat Transfer Correlation in IC Engines, SAE Paper, No. 2008-01-1816, 2008.
[9] R.T.M. Junior, C.R.P. Belchior, Analysis of Different Correlations for Heat Transfer to the Cylinder Wall in Spark-ignition Engines With a Generalized Computational Algorithm, SAE Paper, No. 2008-36-0187, 2008.
[10] H. Mizuno, K. Ashida, A. Teraji, K. Ushijima, S. Takemura, Transient Analysis of Piston Temperature with Consideration of In-cylinder Phenomena Using Engine Measurement and Heat Transfer Simulation Coupled with Tree-dimensional Combustion Simulation, SAE Paper, No. 2009-01-0187, 2009.
[11] J.B. Heywood, Internal Combustion Engine Fundamentals. McGraw-Hill, New York, 1988, pp. 668–683, 690–692.
[12] Y. Harigaya, F. Toda, M. Suzuki, Local Heat Transfer on Combustion Chamber Wall of a Spark Ignition Engine, SAE Paper, No. 931130, 1993, pp. 1567–1575.
[13] S.B. Han, Y.J. Chung, Y.J. Kown, S. Lee, Empirical Formula for Instantaneous Heat Transfer Coefficient in a Spark Ignition Engine, SAE Paper, No. 972995, 1997, pp. 219–226.
[14] A.P. Kleemann, A.D. Gosman, K.B. Binder, Heat transfer in diesel engines: a CFD evaluation study, in: Proceedings of the Fifth International Symposium on Diagnostic and Modeling of Combustion in Internal Combustion Engines, Comodia, Nagoya, 2001, pp. 123–131.
[15] C.D. Depcik, D. Assanis, A Universal Heat Transfer Correlation for Intake and Exhaust Flows in a Spark-ignition Internal Combustion Engine, SAE Paper, No. 2002-01-0372, 2002.
[16] J.H. Grau, J.M. Garcia, J.P. Garcia, A.V. Robles, R.R. Pastor, Modeling Methodology of a Spark-ignition Engine and Experimental Validation Part I: Single-zone Combustion Model, SAE Paper, No. 2002-01-2193, 2002.
[17] P. Zeng, R.G. Prucka, Z.S. Filipa, D.N. Assanis, Reconstructing cylinder pressure of a spark-ignition engine for heat transfer and heat release analyses, in: Proceedings of ICE Division of ASME, Fall Technical Conference, Long Beach, CA, USA, 2004, pp. 1–11.
[18] G.F. Hohenberg, Advanced Approaches for Heat Transfer Calculations, SAE Paper No. 790825, 1979.
[19] A. Mohammadi, M. Yaghoubi, M. Rashidi, Analysis of local convective heat transfer in a spark ignition engine. International Communication in Heat and Mass Transfer 33 (2008) 215–224.
[20] B.E. Launder, P.B. Spalding, The numerical computation of turbulent flows. Computer Method in Applied Mechanics and Engineering 3 (1974) 269–289.
[21] S.K. Hannani, A. Jafari, Determination of temperature in combustion chamber of an internal combustion engine, in: Proceedings of the Fifth Conference in Mechanical Engineering, Rasht, Iran, 2001, pp. 59–65.
[22] B.E. Launder, D.B. Spalding, Mathematical Models of Turbulence. Academic Press, New York, 1972.
[23] D.B. Spalding, Development of eddy-breakup model of turbulent combustion, in: 16th Symposium on Combustion, p. 1657, 1976.
[24] G. Woschni, A Universal Applicable Equation for the Instantaneous Heat Transfer Coefficient in the Internal Combustion Engine, SAE Paper, No. 670913, 1963.
[25] A. Mohammadi, M. Rashidi, Analysis of combustion and heat transfer in a SI engine, in: Second Conference of combustion, Mashhad, Iran, 2004.
[26] P.G. Aleiferie, A.M.K.P. Taylor, K. Ishii, Y. Urata, The nature of early flame development in a lean-burn stratified-charge spark-ignition engine. Combustion and Flame 136 (2004) 283–302.
[27] S.R. Turns, An Introduction to Combustion. McGraw-Hill, New York, 1996, pp. 399–400.